Journal of Photochemistry and Photobiology A: Chemistry 203 (2009) 137–144

Contents lists available at ScienceDirect

Journal of Photochemistry and Photobiology A: Chemistry

journal homepage: www.elsevier.com/locate/jphotochem

# Photocatalytic growth of CdS, PbS, and $Cu_xS$ nanoparticles on the nanocrystalline $TiO_2$ films

Maxim A. Zhukovskiy[a,1], Alexander L. Stroyuk[b,*], Vitaliy V. Shvalagin[b,2], Natalia P. Smirnova[a,1], Oksana S. Lytvyn[c], Anna M. Eremenko[a,1]

[a] Chuiko Institute of Surface Chemistry of Ukr. Nat. Acad. Sci., 17 General Naumov str., 03164 Kyiv, Ukraine
[b] Pysarzhevski Institute of Physical Chemistry of Ukr. Nat. Acad. Sci., 31 Nauky av., 03028 Kyiv, Ukraine
[c] Lashkarev Institute of Semiconductor Physics of Ukr. Nat. Acad. Sci., 41 Nauky av., 03028 Kyiv, Ukraine

ARTICLE INFO

*Article history:*
Received 12 November 2008
Received in revised form
22 December 2008
Accepted 12 January 2009
Available online 21 January 2009

*Keywords:*
Semiconductor nanoparticles
Photocatalysis
Photosynthesis
Titanium dioxide
Cadmium sulfide
Lead sulfide
Copper sulfide
Nanocomposites

ABSTRACT

The $CdS/TiO_2$, $PbS/TiO_2$, and $Cu_xS/TiO_2$ nanocomposites were synthesized via the photocatalytic reduction of sulfur on the surface of nanocrystalline $TiO_2$ films. The photocatalytic synthesis produced smaller CdS nanoparticles in the comparison with the conventional chemical deposition of cadmium sulfide. The mean size of CdS nanoparticles can be varied by changing the illumination intensity and the $TiO_2$ film calcination temperature.

An AFM study of the surface structure of $CdS/TiO_2$ and $PbS/TiO_2$ nanocomposites showed that the photocatalytic deposition results in formation of the polycrystalline 7–80 nm (CdS) or 20–30 nm (PbS) long nanorods. Spatial separation of the photogenerated charge carriers in $CdS/TiO_2$ and $PbS/TiO_2$ nanocomposites was assumed to be the driving force of the formation of such elongated metal sulfide nanoparticle agglomerates.



## 1. Introduction

Large-scale fundamental and applied studies of nanocrystalline titanium dioxide films deposited on the surface of glass, metals, wood, fabric, organic polymers and other materials are stimulated by wide perspectives of the application of such composite materials in various modern technologies [1–5]. These include superhydrophilization of the surfaces and production of self-cleaning materials, formation of the photosensitive coatings on glass elements of living and industrial buildings, production of the highly efficient photoelectro-chemical cells for solar energy storage, the gas sensors technology, etc.

Among the various applications of nanocrystalline $TiO_2$ films of special interest are those based on the photoinduced processes [1–5]. High chemical activity of radical intermediates produced at the light absorption by $TiO_2$ nanoparticles (NPs) is the reason under their unparalleled photocatalytic activity in the oxidation of volatile organic compounds as well as the redox-conversion of small molecules (CO, $NO_x$, $H_2S$, etc.) [6,7].

Further advancement of the photocatalytic systems based on thin porous nanocrystalline $TiO_2$ films is usually associated with their sensitization to the visible light as well as reduction of the undesirable recombinational losses of photogenerated charge carriers [1,2,4]. A combined solution of the two tasks can be provided by the utilization of binary systems containing, along with the nanocrystalline titania, a second light-sensitive component—a dye-sensitizer or a narrow-band-gap semiconductor, the latter having more negative, than $TiO_2$, conduction band edge potential.

In the first case, a photoexcited dye molecule can extremely fast (as fast as $\sim 10^{-15}$ to $10^{-13}$ s) inject an electron into the conduction band of $TiO_2$ NPs [2,3]. The back electron transfer usually takes place in the inverted Marcus region [2,3] and is therefore considerably retarded ($\sim 10^{-6}$ to $10^{-5}$ s), making the charge carriers separation almost irreversible.

Spatial charge carriers separation in the composite systems of the second type is achieved through the interfacial transfer of a photogenerated electron from the narrow-band-gap component into the conduction band of titanium dioxide. The most promising results have been achieved with metal-sulfide semiconductors

* Corresponding author. Tel.: +380 44 525 0270; fax: +380 44 525 6662.
*E-mail addresses:* stroyuk@inphyschem-nas.kiev.ua, alstroyuk@ukr.net (A.L. Stroyuk), annaerem@ukr.net (A.M. Eremenko).
[1] Tel.: +380 44 4229698.
[2] Tel.: +380 44 525 0270; fax: +380 44 525 6662.

1010-6030/$ – see front matter © 2009 Elsevier B.V. All rights reserved.
doi:10.1016/j.jphotochem.2009.01.007

MS–CdS, PbS, $Bi_2S_3$, $MoS_2$, $Bi_2S_3$, as sensitizers for $TiO_2$. For example, the visible light photoexcitation of binary systems composed of CdS and $TiO_2$ NPs results in the fast ($\sim 10^{-12}$ to $10^{-11}$ s [8–11]) electron transfer from cadmium sulfide to the $TiO_2$ conduction band, the process successfully competing with the radiative electron-hole recombination ($\sim 10^{-10}$ to $10^{-9}$ s for CdS NPs [10]), which is clearly demonstrated by the quenching of CdS luminescence in CdS–$TiO_2$ binary systems [8,11–14]. According to [13], the quantum efficiency of interfacial electron transfer from CdS to $TiO_2$ is close to 100%.

Fast spatial separation of opposite charge carriers in CdS/$TiO_2$ nanostructures is one of the reasons for their advanced photocatalytic activity in various reactions: water reduction to hydrogen [15–17], the decomposition of organic dyes [18–21] and tetrachlorobenzene [22], reduction of methylviologen [13,23], oxidation of indole [24], etc. Considerable photocatalytic activity in water reduction was also reported for $Cd_xZn_{1-x}S/TiO_2$ nanostructures [25]. Composite $Bi_2S_3/TiO_2$ nanostructures were found to possess photocatalytic activity in the visible-light-driven destruction of organic dyes [20]. The deposition of CdS [26–32], $WS_2$ [33], PbS [29,34–37], $Bi_2S_3$ [29,38], $Sb_2S_3$ and $Ag_2S$ [29], $CuInS_2$ [39] NPs both inside the pores and on the outer surface of nanocrystalline $TiO_2$ films produces visible-light-sensitive photoelectrodes for solar cell applications.

Along with the traditional synthesis of MS/$TiO_2$ nanocomposites such as the chemical bath deposition, new photochemical approaches are being currently developed exploiting the capability of $TiO_2$ NPs to photocatalytically transform sulfur-containing compounds [25,40,41]. Photosynthesized MS/$TiO_2$ nanostructures are generally characterized by a smaller sulfide NP size and a better electronic contact between the components of the nanocomposite favoring their application as binary photocatalysts. For example, $MoS_2/TiO_2$ and $WS_2/TiO_2$ nanostructures prepared at the photocatalytic decomposition of $MoS_4^{2-}$ and $WS_4^{2-}$ on the surface of $TiO_2$ demonstrate high photocatalytic activity in 4-chlorophenol and methylene blue oxidation [40], as well as hydrogen evolution from aqueous sodium sulfide/sodium sulfite solutions [41]. Ternary CdS/$Au^0$/$TiO_2$ nanocomposites produced at the photocatalytic sulfur reduction over composite $Au^0/TiO_2$ NPs in the presence of $Cd^{II}$ possess remarkable photocatalytic activity in methylviologen reduction [42].

Here we report on the utilization of photocatalytic reduction of $S_8$ by ethanol on the surface of nanocrystalline titanium dioxide films for the preparation of binary MS/$TiO_2$ nanocomposites, where MS = CdS, PbS, $Cu_xS$. It was shown that favorable conditions for the spatial charge carriers separation in CdS/$TiO_2$ and PbS/$TiO_2$ nanostructures can lead to the formation of metal-sulfide nanoagglomerates with anisotropic shape. In case of CdS/$TiO_2$ nanocomposite the basic factors determining the size and optical properties of photoproduced CdS NPs were examined.

## 2. Experimental

Titanium(IV) tetraisopropoxide, Pluronic 123, acetylacetone, concentrated HCl (36.6 wt.%), sulfur, thiourea, $Cd(CH_3COO)_2$, $Pb(CH_3COO)_2$, and $CuCl_2$ of reagent grade purity were purchased from Aldrich and used without additional purification.

Nanocrystalline $TiO_2$ films on glass substrates were prepared similarly to [43], using titanium(IV) tetraisopropoxide, triblock-copolymer Pluronic 123 as a template and hydrochloric acid as a sol–gel transition catalyst. The primary films were deposited onto glass plates from a colloidal solution by the "dip-coating" method

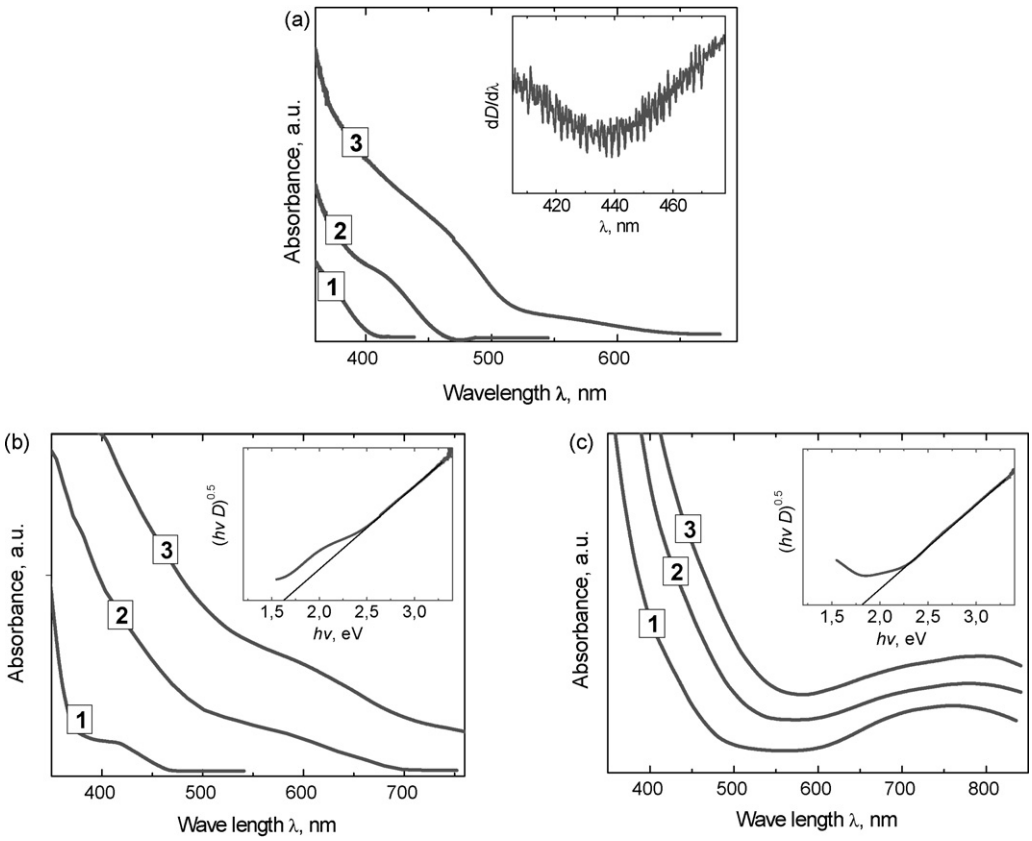


**Fig. 1.** (a) Absorption spectra of a nanocrystalline $TiO_2$-6 film (curve 1) as well as CdS/$TiO_2$ films produced by the photocatalytic (curve 2) and chemical (curve 3) deposition of CdS. *In the inset*: the first-order derivative of the curve 2. (b and c) Absorption spectra of the PbS/$TiO_2$-6 (b) and $Cu_xS/TiO_2$-6 (c) nanostructures after 2 (1), 6 (2), and 6 min (3) illumination. *In the insets*: the spectral curves (3) presented as $(h\nu \times D(\lambda))^{0.5} - h\nu$ dependences, where $h\nu$ and $D(\lambda)$ are the light quantum energy and the optical density of the film on the wavelength $\lambda$, respectively.

and dried at 100 °C. The procedure was repeated several (up to six) times to produce titania coatings of increasing thickness. The corresponding films are hereinafter referred to as $TiO_2$-$x$ ($x$ = 1–6), where $x$ is a number of "dip-coating" cycles. The dried films were calcined at 350, 400 or 500 °C.

The chemical synthesis of composite CdS/$TiO_2$ films can be summarized as follows. A $TiO_2$ film was immersed in an aqueous solution of cadmium(II) acetate and thiourea and then pH was raised to 12–13 with ammonia. Cadmium sulfide NPs were deposited onto the surface of a nanocrystalline $TiO_2$ film as a result of the reaction between $Cd^{II}$ and $HS^-$, the latter releasing at the basic hydrolysis of thiourea.

The absorption spectra of films were recorded on the Specord 210 spectrophotometer. Atomic force microscopy (AFM) experiments were carried out on the Nanoscope IIIa setup. Illumination of $TiO_2$ films dipped into ethanol solutions of a metal salt ($1 \times 10^{-3}$ M) and $S_8$ ($1 \times 10^{-3}$ M in terms of atomic sulfur) was carried out in cylindrical glass reactors after pumping out the air. A high-pressure 1000 W mercury lamp equipped with optical filters was used as a light source with a narrow spectral window 310–370 nm with the dominant wave length $\lambda_{max}$ = 365 nm. The irradiation intensity was measured by the ferrioxalate actinometer and used in the determination of the quantum yields of the photocatalytic reactions.

The rate ($V$) of the photocatalytic deposition of CdS was measured as an increase in the optical density of a film sample at voluntarily chosen wavelength (410 nm) after 20 min illumination.

## 3. Results and discussion

### 3.1. Synthesis and optical properties of MS/$TiO_2$ nanocomposites

Illumination of the nanocrystalline $TiO_2$ films dipped into evacuated alcohol solutions of a metal salt ($Cd(CH_3COO)_2$, $Pb(CH_3COO)_2$ or $CuCl_2$) and sulfur results in a change in the film color as the metal sulfide is deposited onto the film surface. No photoinduced coloration changes were observed in the absence of $TiO_2$ films or with the original glass plates, indicating the sulfide deposition to be exclusively of photocatalytic character. Neither signs of the presence of metal sulfides in the solution after the extraction of the $TiO_2$ films were observed indicating that cadmium, lead, and copper sulfides were firmly attached to the surface of the photocatalyst films.

Fig. 1a presents the absorption spectra of an original $TiO_2$-6 film (curve 1) as well as the CdS/$TiO_2$ films (curves 2 and 3). The long-wave edges of CdS/$TiO_2$ nanocomposites produced photocatalytically (curve 2) and chemically (curve 3) can be observed at 461–463 and 515–517 nm, implying the band gap $E_g$ of CdS NPs being 2.68–2.69 and 2.40–2.41 eV, respectively.

To evaluate from the optical data the size ($2R$) of CdS NPs deposited a comparative analysis of the experimental data on the correlation between $E_g$ and $2R$ obtained by the transmission electronic microscopy [44–47] and X-rays diffraction [48,49], as well as theoretical modelling of this correlation [50–56] was carried out. It revealed that almost all the experimental data in a wide (3–20 nm) range of the CdS NPs size can be described by the effective masses approximation using the well-known expression (1) [51,53,57].

$$\Delta E_g = \frac{\hbar^2 \pi^2}{2R^2}\left[\frac{1}{m_e^* m_0} + \frac{1}{m_h^* m_0}\right] \quad (1)$$

where $\Delta E_g = E_g - E_g^{bulk}$, $E_g^{bulk}$ is the band gap of bulk cubic cadmium sulfide (2.4 eV), $\hbar$ is the reduced Planck constant, $m_e^*$ ($m_h^*$) is the effective mass of conduction band electron $e_{CB}^-$ (valence band hole $h_{VB}^+$), $m_0$ is the electron rest mass. It should be noted that different values of $m_e^*$ (0.18 [52,58], 0.19 [51], 0.204 [59]) and $m_h^*$ (0.53 [52,55,58], 0.70 [59], 0.80 [51]) have been reported in the literature, but the error of $2R$ determination induced by this scatter of values within the range of the most frequent $E_g$ values (2.45–2.90 eV) does not exceed 5% and can be therefore neglected when applying equation (1) to estimate the size of CdS NPs.

It was shown that the size of chemically deposited CdS particles is larger than 15–20 nm, their band gap being almost equal to that of bulk cadmium sulfide. At the same time, the photocatalytic CdS deposition results in the formation of smaller, 6.1–6.2 nm, CdS NPs.

It should be noted that estimations using the absorption threshold of photochemically produced CdS NPs can give somewhat overrated size values due to larger NPs contributing more substantially into the absorption band edge of the CdS NPs ensemble as compared with the smaller ones. More reasonable size value can be obtained from the position of the first excitonic maximum of CdS NPs, the latter appearing distinctly on the first-order derivative of the absorption spectrum (see Inset in Fig. 1a). The average size of CdS NPs estimated from the excitonic maximum at 438–440 nm is 5.1–5.2 nm. The difference between the size values derived from the absorption threshold and the first excitonic maximum can be then regarded as an estimate of the size dispersion of photocatalytically produced CdS NPs (~20%).

The visible light absorption by lead (Fig. 1b) and copper (Fig. 1c) sulfides increases gradually in the course of the illumination and originates from the indirect interband electronic transitions [57,59]. This type of transitions is characterized by structureless absorption bands descending smoothly towards the long-wave side of the spec-

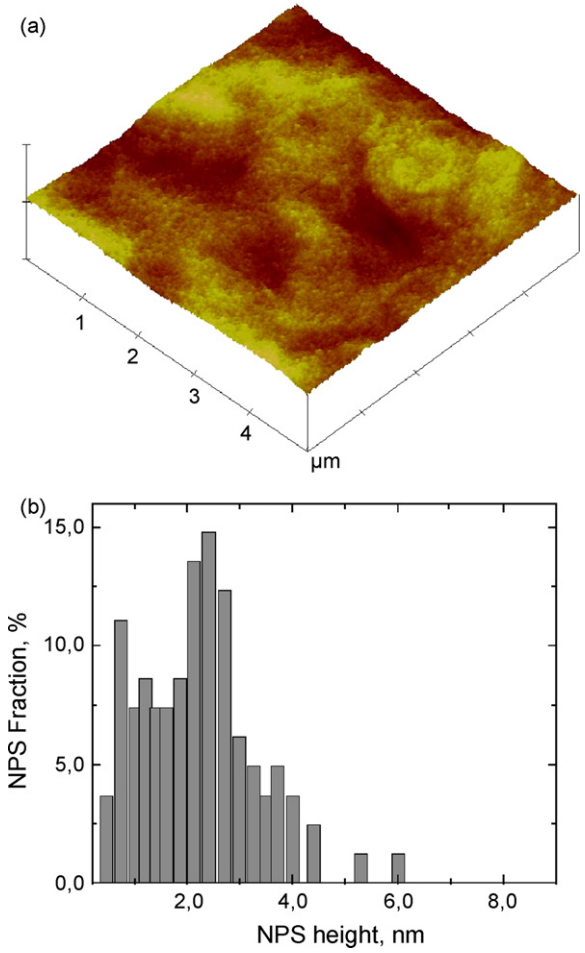


**Fig. 2.** (a) The AFM image of a 5 μm × 5 μm surface area of a $TiO_2$-6 film. The film calcination temperature is 400 °C. The vertical scale is 100 nm. (b) The $TiO_2$ NPs height distribution chart (plotted after 100 separate measurements).

trum, the fact making it impossible to determine $E_g$ directly from the optical spectra. Absorption coefficient $\alpha$ of indirect semiconductors (proportional to the optical density of a sample $D$) can be expressed as a function (2) of the light energy $h\nu$ [57]

$$D = A\frac{(h\nu - E_{in})^2}{h\nu} \quad (2)$$

where $E_{in}$ is an energy of indirect transition equal to $E_g \pm E_f$, $E_f$ is a phonon energy, $A$ is a constant. As the values of $E_f$ do not usually exceed $10^{-2}$ eV [57,59], the condition $E_g \gg E_f$ is valid allowing to neglect $E_f$ and assume $E_{in} \approx E_g$.

The insets in Fig. 1b and c show the absorption spectra of PbS/$TiO_2$-6 and $Cu_xS$/$TiO_2$-6 nanocomposites presented as $(D \times h\nu)^{0.5} - h\nu$ dependences. Extending linear sections of the spectra to the abscissae axis one can obtain the band gaps of the sulfide NPs $E_g$(PbS) = 1.63–1.64 eV and $E_g$($Cu_xS$) = 1.82–1.83 eV. Gradual growth of the near-IR absorption tail in case of $Cu_xS$/$TiO_2$ nanocomposite (Fig. 1, curve 4) is typical for non-stoichiometric $Cu_xS$ NPs with $1 < x < 2$ [60–63].

An analysis of the reported experimental [64–66] and theoretical [64,67–69] data concerning the correlation between the size and the band gap of PbS NPs showed that the equation (1), though being quite valid for CdS NPs, cannot be applied for the correct determination of the size of PbS NPs. At the same time, the latter can be reliably determined from the optical data using alternative theoretical models, such as a hyperbolic bands model [64], a four-band-envelope formalism [67], or the effective mass approximation with the finite-depth potential well [69], which give good agreement with the experimental results in the range $E_g$ = 0.5–2.5 eV. The average size of the photocatalytically deposited PbS NPs calculated using the above-mentioned theoretical correlations was found to be $2R$ = 3.7–3.8 nm.

No reliable data were found concerning the $E_g$–$2R$ correlations for copper sulfide materials. In this view, to estimate the size of the photocatalytically deposited $Cu_xS$ NPs an $E_g$–$R$ correlation obtained by an indirect method [63] was applied. The average size of $Cu_xS$ NPs was found to be 8–10 nm. This value should however be treated cautiously due to the fact that the band gap of $Cu_xS$ NPs can be affected not only by size effects but also by the phase composition of non-stoichiometric copper sulfide, some of the phases having comparatively large $E_g$ (for example, 2.3 eV for $Cu_{1.8}S$ [59]).

### 3.2. The surface morphology of CdS/$TiO_2$, PbS/$TiO_2$ and $Cu_xS$/$TiO_2$ nano-composites

Fig. 2 presents an AFM image of the surface of a nanocrystalline $TiO_2$-6 film (a) and the NPs height distribution diagram (b) derived from the image (a). The average roughness of the surface area studied was found to be 2–3 nm, with some $TiO_2$ NPs being as high as 6 nm. Fig. 3a shows that the film retains the relief uniformity after the chemical deposition of cadmium sulfide, its average roughness increasing to 3–5 nm (Fig. 3b).

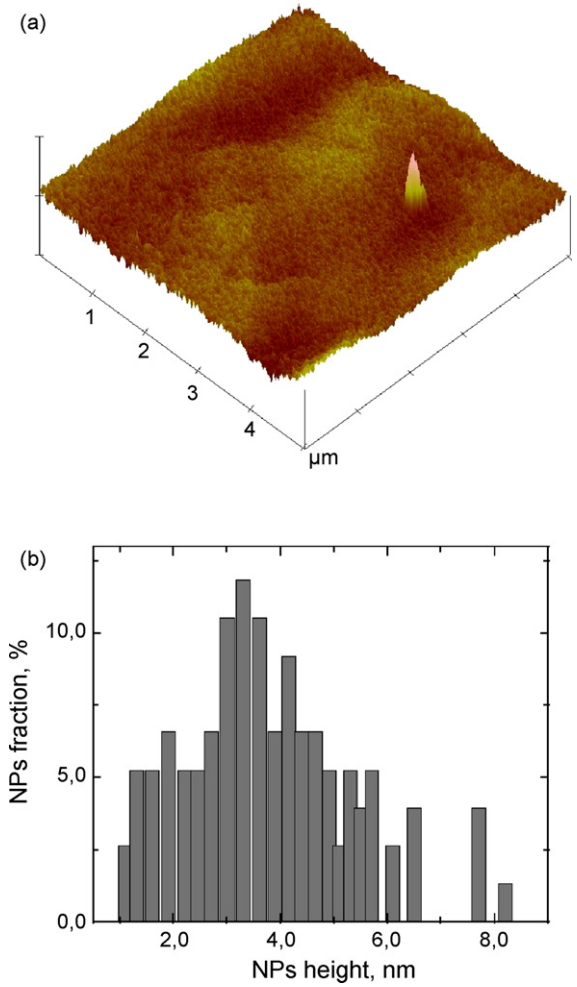


**Fig. 3.** (a) The AFM image of a 5 μm × 5 μm surface area of the CdS/$TiO_2$-6 nanocomposite, prepared by the chemical deposition of cadmium sulfide. The vertical scale is 100 nm. (b) The CdS NPs height distribution chart (plotted after 100 separate measurements).

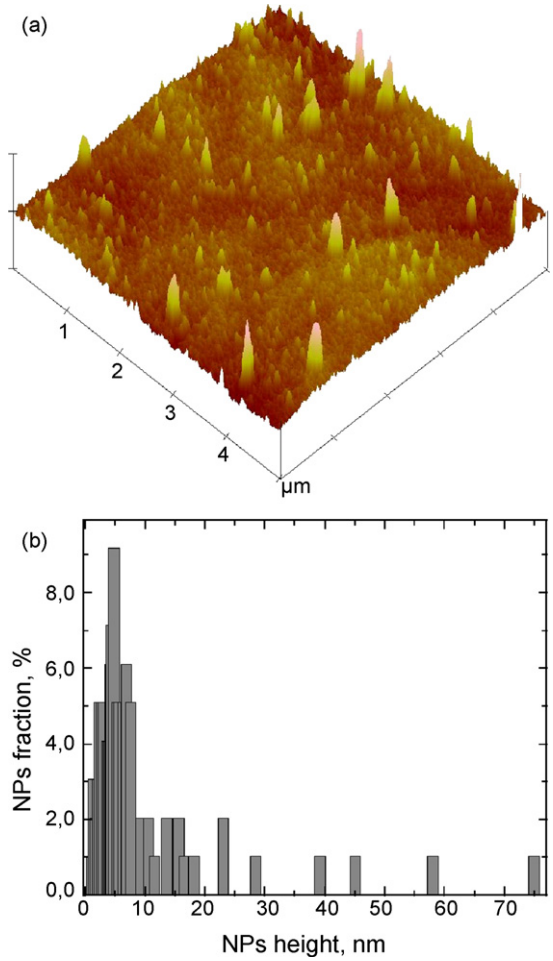


**Fig. 4.** (a) The AFM image of a 5 μm × 5 μm surface are of the CdS/$TiO_2$ nanocomposite, prepared by the photocatalytic deposition of cadmium sulfide on the surface of a $TiO_2$-6 film in the presence of $Cd(CH_3COO)_2$. The vertical scale is 100 nm. (b) The CdS NPs height distribution chart (plotted after 100 separate measurements).

The surface morphology of the photocatalytically produced CdS/$TiO_2$ films is drastically different (Fig. 4a). The figure shows that the photocatalytic reduction of sulfur in the presence of $Cd(CH_3COO)_2$ on a $TiO_2$-6 film results in the formation of elongated rod-like CdS nanoagglomerates with the height ranging from 10 to 75 nm (Fig. 4b). In places not occupied by the agglomerates the average height of CdS NPs is 3–6 nm. The average roughness of these areas was found to be 2–3 nm, similarly to the original $TiO_2$ film. It can be therefore concluded that the bulk of cadmium sulfide is photodeposited as the rod-like nanoagglomerates, not affecting the rest of the film surface.

It has been shown recently [70] that the photocatalytic CdS deposition in similar systems containing ZnO nanorods with the length 100–350 nm and the diameter 20–150 nm produces polycrystalline CdS nanotubes being as long as 0.5–0.8 μm with the inner diameter 15–110 nm replicating the diameter of original ZnO nanorods. The mechanism of the process has been proposed, considering the spatial charge carriers separation between the ZnO nanorod tips and attached CdS NPs as a driving force behind the formation of CdS nanotubes. The CdS nanorods formation in the systems presently under study can be accounted for by a similar mechanism.

Light absorption by a nanocrystalline $TiO_2$ film produces (at $h\nu > E_g$) conduction band electrons and valence band holes. The electrons react with the adsorbed sulfur [42], while the holes oxidize ethanol molecules to $CH_3C^{\bullet}HOH$ radicals (Fig. 5, step I). The alcohol radical can readily inject the second electron into the $TiO_2$ conduction band while being oxidized to acetaldehyde [1].

Not only $TiO_2$ but also CdS/$TiO_2$ composite NPs can participate in the photocatalytic process after the primary CdS NPs being deposited onto the $TiO_2$ film (Fig. 5, step II). The energy diagram given in Fig. 5 describes the bulk CdS/$TiO_2$ system using the well-known values $E_g^{bulk}(CdS) = 2.4$ eV, $E_g^{bulk}(TiO_2) = 3.2$ eV, as well as the conduction band potentials $E_{CB}^{bulk}(CdS) = -0.8$ V vs normal hydrogen electrode (NHE) and $E_{CB}^{bulk}(TiO_2) = -0.3$ V vs NHE (pH 7) [1,11]. The diagram shows that even in the bulk system, i.e. irrespective of possible quantum size effects in the photodeposited CdS NPs, there exist very favorable conditions for the photoinduced spatial charge carriers separation. Substantial energy gap between the edges of the corresponding bands in CdS and $TiO_2$ ($\Delta E_{CB} = 0.5$ eV, $\Delta E_{VB} = 1.3$ eV) favors to fast and irreversible separation of the electrons and holes between the components of the CdS/$TiO_2$ composite. The reductive and oxidative branches of the photocatalytic reaction appear therefore spatially separated, the sulfur reduction and CdS formation proceeding predominantly on the $TiO_2$ surface, while the ethanol oxidation taking place on CdS NPs (Fig. 5, step II). The Coulomb interaction between the electron and hole is expected to keep them close to the CdS–$TiO_2$ interface, thus enabling the photocatalytic $S_8$ reduction and cadmium sulfide deposition exactly at the site of the contact between CdS NPs and $TiO_2$ film. Such a mechanism can account for the formation of rodelike agglomerates consisting of separate CdS NPs (Fig. 5, step III). It should be noted that the proposed mechanism has similar features with the mechanism of catalytic formation of carbon nanotubes, where the nanotube growth proceeds on the interface between the carbon nanotube and a catalyst nanocrystal at the expense of the oxidation of a gaseous substrate [71].

The surface morphology, which is close to that of the photosynthesized CdS/$TiO_2$ nanocomposites, can be also observed in case of nanocrystalline PbS/$TiO_2$ films (Fig. 6). The height of the elongated PbS NP aggregates was found to be 20–30 nm. The mechanism of the formation of anisotropic PbS NP nanoaggregates on the surface of a $TiO_2$ film is apparently the same as in the case of cadmium sulfide. Lead sulfide NPs, similarly to CdS NPs, were shown to possess photocatalytic properties [65,72,73]. There are also examples of efficient spatial charge separation resulting in increased photocurrent and spectral sensitization of a $TiO_2$ substrate in the photovoltaic systems based on PbS/$TiO_2$ nanocomposites [29,34–37].

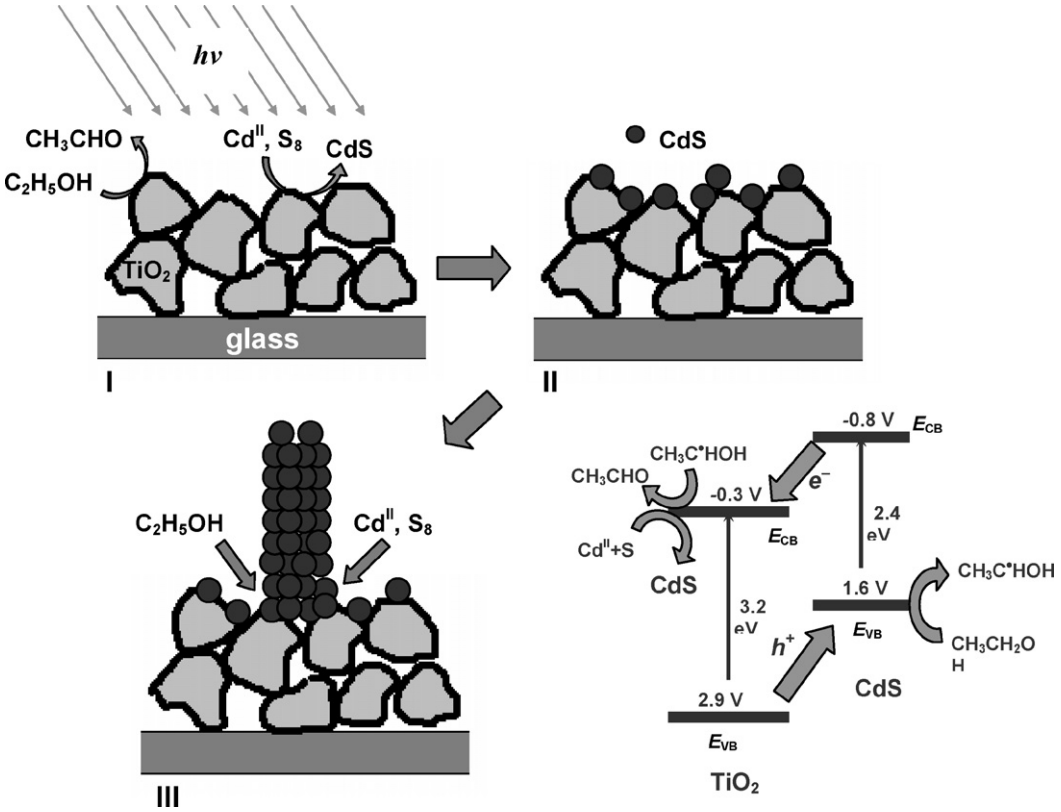


**Fig. 5.** A scheme illustrating the photocatalytic formation of polycrystalline CdS nanorods on the surface of $TiO_2$ films and the photoinduced charge separation between cadmium sulfide and titanium oxide.

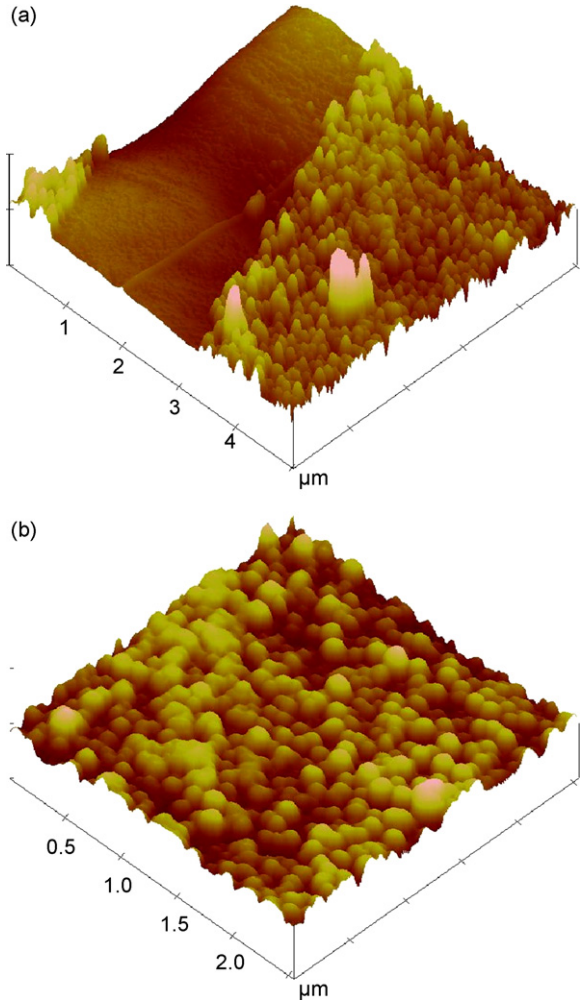


**Fig. 6.** The AFM images of 5 × 5 (a) and 2.5 × 2.5 μm (b) surface areas of a PbS/$TiO_2$ nanocomposite produced by the photocatalytic sulfur reduction on the surface of a $TiO_2$-6 film in the presence of $Pb(CH_3COO)_2$. The vertical scales are 100 (a) and 50 nm (b).

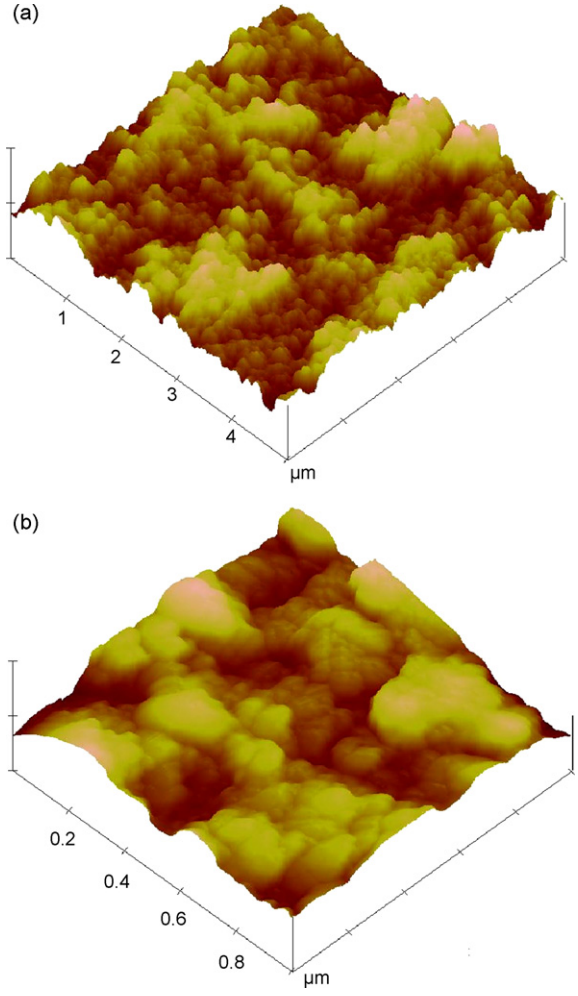


**Fig. 7.** The AFM images of 5 × 5 (a) and 1 × 1 μm (b) surface areas of a $Cu_xS/TiO_2$ nanocomposite prepared by the photocatalytic sulfur reduction on the surface of a $TiO_2$-6 film in the presence of $CuCl_2$. The vertical scales are 100 (a) and 50 nm (b).

Smaller height of PbS NPs and the average surface roughness of PbS/$TiO_2$ nanocomposites increased to 6–7 nm as compared to the original $TiO_2$-6 film, indicate more uniform, than CdS, deposition of lead sulfide NPs onto the surface of $TiO_2$. The fact can be accounted for by the lower photocatalytic activity of PbS/$TiO_2$ nanoheterostructure in the comparison with that of CdS/$TiO_2$ nanocomposite.

Fig. 7 shows that copper sulfide is deposited on the $TiO_2$ surface in a substantially agglomerated form. The mean roughness of composite $Cu_xS/TiO_2$ films was found to be as high as 60 nm, the lateral dimensions of separate agglomerates reaching 250 nm. The lack of directional growth of $Cu_xS$ NPs may reflect unfavorable conditions for the spatial separation of the photogenerated charge carriers in $Cu_xS/TiO_2$ nanostructure. The results are in accordance with the reported data on the photochemical inactivity of $Cu_xS$ NPs and low efficiency of the charge carriers separation in $Cu_xS/TiO_2$ nanocomposites.

### 3.3. *Factors affecting the average size of CdS NPs and the rate of photocatalytic formation of CdS/$TiO_2$ nanocomposites*

Among the nanocomposites under discussion, CdS/$TiO_2$ has apparently the greatest potential of application as a photocatalyst of various redox-reactions. As a rule, the effectiveness of the interfacial electron transfer from cadmium sulfide to $TiO_2$ increases as CdS NPs size decreases, due to an expansion of the energy gap between the conduction band edges of both semiconductors and more intimate electronic contact between the $TiO_2$ surface and size-quantized CdS NPs. In this connection, of special interest are the means of tailoring the size of CdS NPs and, therefore, of controlling the electronic parameters of CdS/$TiO_2$ nanocontacts. An analysis of spectral properties of nanocrystalline CdS/$TiO_2$ films produced under different conditions of the photocatalytic experiment as well as from $TiO_2$ films of different history showed that the basic parameters allowing size variation of the photodeposited CdS NPs are the irradiation intensity and the temperature of $TiO_2$ films calcination.

The rate of the photocatalytic process ($V$) was found to grow in the direct proportion to the intensity of the light flux ($I$) (Fig. 8). The absorbance threshold of CdS NPs produced on the surface of $TiO_2$-6 films after 80 min irradiation with $I = 5.6 \times 10^{17}$ quanta per min, 461–463 nm (Fig. 8, curve 1 in the inset) corresponds to $E_g$ = 2.68–2.69 eV and $2R$ = 6.1–6.2 nm. At the same time, the photocatalytic deposition yields CdS NPs with $E_g$ = 2.51–2.52 eV and $2R$ = 9.2–9.4 nm, when carried out at $I = 2.8 \times 10^{17}$ quanta per min. Lowering of the average size of NPs deposited on the surface of $TiO_2$ samples with increasing the light intensity is often observed, for example, at the photocatalytic deposition of metal NPs [74] and is usually accounted for by the growth of primary nuclei number at higher photon fluxes.

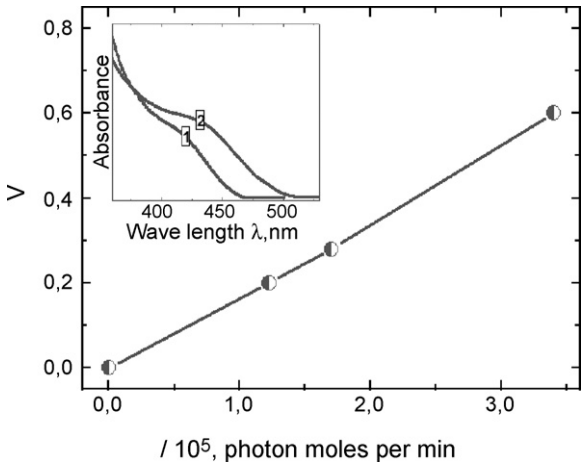


**Fig. 8.** The rate of photocatalytic deposition of CdS NPs ($V$) on the surface of a $TiO_2$-6 film vs the irradiation intensity $I$. *The inset*: Normalized absorption spectra of the CdS/$TiO_2$ nanocomposites prepared at $I = 5.6 \times 10^{17}$ (1) and $2.8 \times 10^{17}$ quanta per min (2). $[Cd(CH_3COO)_2] = [S] = 1 \times 10^{-3}$ M, the $TiO_2$ film calcination temperature is 400 °C.

The photocatalytic reaction rate was found to increase threefold with increasing the thickness and light absorbance of the films from $TiO_2$-1 to $TiO_2$-6 samples (Fig. 9). Judging by the optical properties of CdS deposited, the average NPs size remains at that quite constant, varying from 5 to 6 nm with the illumination time.

The size and optical properties of CdS NPs were found to vary along with the preparation history of the $TiO_2$ film used, the primary factor being the film calcination temperature $T_c$. The average size of CdS NPs produced after 20 min irradiation is 4.8–4.9 nm for a $TiO_2$-6 film calcined at $T_c = 350$ °C, 5.5–5.6 nm for $T_c = 400$ °C, and 5.8–5.9 nm for $T_c = 500$ °C. The increase in the calcination temperature of $TiO_2$ films synthesized using Pluronic 123 had been earlier found to promote elimination of the organic template out of the film pores and the hydrophilization of the film surface, the wetting angle of the film decreasing from 23° for $T_c = 350$ °C to 10° for $T_c = 500$ °C [75]. The fact can be accounted for by an increase in the number of structural defects promoting the dissociative water adsorption with increasing $T_c$ [76,77]. Growth of the polarity of the film surface can favor cadmium sulfide deposited in the course of the photocatalytic reaction to form larger NPs, as is the case for colloidal semiconductor solutions when water is used instead of less polar organic solvents [57].

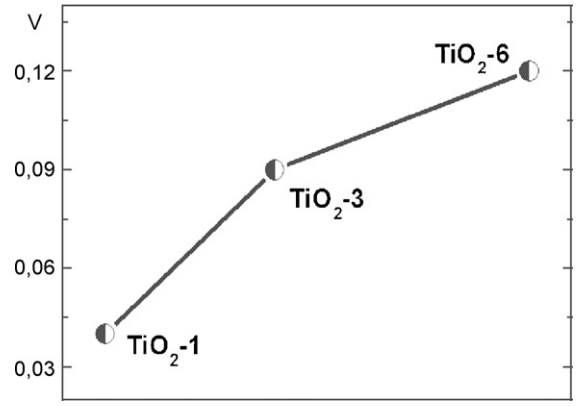


**Fig. 9.** The rate of the photocatalytic CdS deposition vs the thickness of an original $TiO_2$ film. The $TiO_2$ film calcination temperature is 400 °C, $I = 5.6 \times 10^{17}$ quanta per min, $[Cd(CH_3COO)_2] = [S] = 1 \times 10^{-3}$ M.

## 4. Conclusions

The photocatalytic reduction of sulfur by ethanol on the surface of nanocrystalline $TiO_2$ films was found to lead to the formation of CdS/$TiO_2$, PbS/$TiO_2$, and $Cu_xS$/$TiO_2$ nanocomposites incorporating 4–10 nm metal sulfide nanoparticles. Factors, affecting the photodeposition rate and average size of CdS nanoparticles were discussed.

It was shown that the photocatalytic approach proposed allows to prepare CdS/$TiO_2$ with smaller cadmium sulfide nanoparticles in the comparison with the chemical CdS deposition, as well as to vary the nanoparticle size by changing the irradiation intensity and the calcination temperature of a $TiO_2$ film.

An atomic force microscopy study of the surface of CdS/$TiO_2$, PbS/$TiO_2$, and $Cu_xS$/$TiO_2$ nanocomposites showed the products of the photocatalytic deposition of cadmium and lead sulfides to be rod-like 75 nm (CdS) or 30 nm (PbS) nanoaggregates. The polycrystalline CdS and PbS nanorods are oriented normally to the surface of $TiO_2$ films and consist of separate nanometer metal sulfide particles manifesting pronounced quantum confinement effects.

A mechanism of the formation of CdS and PbS nanorods on the surface of nanocrystalline $TiO_2$ films was proposed, assuming the spatial separation of the photogenerated charge carriers between the constituents of CdS/$TiO_2$ and PbS/$TiO_2$ nanocomposites to be the driving force under the growth of elongated agglomerates of metal sulfide nanoparticles.

## References

[1] A. Linsebigler, G. Lu, J. Yates Jr., Chem. Rev. 95 (1995) 735–758.
[2] X. Chen, S. Mao, Chem. Rev. 107 (2007) 2891–2959.
[3] S. Günes, N. Sariciftci, Inorg. Chem. Acta 361 (2008) 581–588.
[4] D. Shchukin, D. Sviridov, J. Photochem. Photobiol. C 7 (2006) 23–39.
[5] A. Fujishima, X. Zhang, D. Tryk, Int. J. Hydrogen En. 32 (2007) 2664–2672.
[6] M. Hoffmann, S. Martin, W. Choi, D. Bahnemann, Chem. Rev. 95 (1995) 69–96.
[7] A. Fujishima, T. Rao, D. Tryk, J. Photochem. Photobiol. C 1 (2000) 1–21.
[8] K. Gopidas, M. Bohorquez, P. Kamat, J. Phys. Chem. 94 (1990) 6435–6440.
[9] J. Blackburn, D. Selmarten, A. Nozik, J. Phys. Chem. B 107 (2003) 14154–14157.
[10] J. Evans, K. Springer, J. Zhang, J. Chem. Phys. 101 (1994) 6222–6225.
[11] D. Duonghong, J. Ramsden, M. Grätzel, J. Am. Chem. Soc. 104 (1982) 2977–2985.
[12] D. Lawless, S. Kapoor, D. Meisel, J. Phys. Chem. 99 (1995) 10329–10335.
[13] L. Spanhel, H. Weller, A. Henglein, J. Am. Chem. Soc. 109 (1987) 6632–6635.
[14] P. Sant, P. Kamat, Phys. Chem. Chem. Phys. 4 (2002) 198–203.
[15] W. So, K. Kim, S. Moon, Int. J. Hydrogen En. 29 (2004) 229–234.
[16] J. Jang, W. Li, S. Oh, J. Lee, Chem. Phys. Lett. 425 (2006) 278–282.
[17] J. Jang, H. Kim, P. Borse, J. Lee, Int. J. Hydrogen En. 32 (2007) 4786–4791.
[18] J. Yu, L. Wu, J. Lin, P. Li, Q. Li, Chem. Commun. (2003) 1552–1553.
[19] Y. Bessekhouad, N. Chaoui, M. Trzpit, N. Ghazzal, D. Robert, J. Weber, J. Photochem. Photobiol. A 183 (2006) 218–224.
[20] Y. Bessekhouad, D. Robert, J. Weber, J. Photochem. Photobiol. A 163 (2004) 569–580.
[21] J. Tristão, F. Magalhães, P. Corio, M. Sansiviero, J. Photochem. Photobiol. A 181 (2006) 152–157.
[22] H. Yin, Y. Wada, T. Kitamura, T. Sakata, H. Mori, S. Yanagida, Chem. Lett. (2001) 334–335.
[23] J. Kim, J. Choi, Y. Lee, J. Hong, J. Lee, J. Yang, W. Lee, N. Hur, Chem. Commun. (2006) 5024–5026.
[24] A. Kumar, A. Jain, J. Photochem. Photobiol. A 156 (2003) 207–218.
[25] S. Tambwekar, D. Venugopal, M. Subrahmanyam, Int. J. Hydrogen En. 24 (1999) 957–963.
[26] L. Peter, D. Riley, E. Tull, K. Wijayantha, Chem. Commun. (2002) 1030–1031.
[27] G. Larramona, C. Choné, A. Jacob, D. Sakakura, B. Delatouche, D. Péré, X. Cieren, M. Nagino, R. Bayón, Chem. Mater 18 (2006) 1688–1696.
[28] T. Toyoda, J. Sato, Q. Shen, Rev. Sci. Instrum. 74 (2003) 297–299.
[29] R. Vogel, P. Hoyer, H. Weller, J. Phys. Chem. 98 (1994) 3183–3188.
[30] E. Hao, B. Yang, J. Zhang, X. Zhang, J. Sun, J. Shen, J. Mater. Chem. 8 (1998) 1327–1328.
[31] R. Mane, M. Yoon, H. Chung, S. Han, Solar Energy 81 (2007) 290–293.
[32] Y. Shen, Y. Lee, Nanotechnology 19 (2008) 045602.
[33] M. Thomalla, H. Tributsch, J. Phys. Chem. B 110 (2006) 12167–12171.
[34] R. Patil, C. Lokhande, R. Mane, T. Gujar, S. Han, J. Non-Crystalline Solids 353 (2007) 1645–1649.
[35] J. Hong, D. Choi, M. Kang, D. Kim, K. Kim, J. Photochem. Photobiol. A 143 (2001) 87–92.
[36] S. Chen, M. Paulose, C. Ruan, G. Mor, O. Varghese, D. Kouzoudis, C. Grimes, J. Photochem. Photobiol. A 177 (2006) 177–184.

[37] P. Wang, L. Wang, B. Ma, B. Li, Y. Qiu, J. Phys. Chem. B 110 (2006) 14406–14409.
[38] L. Peter, K. Wijayantha, D. Riley, J. Waggett, J. Phys. Chem. B 107 (2003) 8378–8381.
[39] M. Nanu, J. Schoonman, A. Goossens, Adv. Func. Mater. 15 (2005) 95–100.
[40] W. Ho, J. Yu, J. Lin, J. Yu, P. Li, Langmuir 20 (2004) 5865–5869.
[41] D. Jing, L. Guo, Catal. Commun. 8 (2007) 795–799.
[42] H. Tada, T. Mitsui, T. Kiyonaga, T. Akita, Nature Mater 5 (2006) 782–786.
[43] Yu. Gnatyuk, N. Smirnova, A. Eremenko, V. Ilyin, Ads. Sci. Technol. 23 (2005) 497–508.
[44] S. Gorer, J. Ganske, J. Hemminger, R. Penner, J. Am. Chem. Soc. 120 (1998) 9584–9593.
[45] K. Murakoshi, H. Hosokawa, M. Saitoh, Y. Wada, T. Sakata, H. Mori, M. Satoh, S. Yanagida, J. Chem. Soc., Faraday Trans. 94 (1998) 579–586.
[46] A. Eychmüller, L. Katsikas, H. Weller, Langmuir 6 (1990) 1605–1608.
[47] F. Wu, J. Yu, J. Joo, T. Hyeon, J. Zhang, Opt. Mater. 29 (2007) 858–866.
[48] T. Vossmeyer, L. Katsikas, M. Giersig, I. Popovic, K. Diesner, A. Chem-seddine, A. Eychmüller, H. Weller, J. Phys. Chem. 98 (1994) 7665–7673.
[49] P. Nandakumar, C. Vijayan, Y. Mutri, J. Appl. Phys. 91 (2002) 1509–1514.
[50] A. Tomasulo, M. Ramakrishna, J. Chem. Phys. 105 (1996) 3612–3626.
[51] L. Brus, J. Chem. Phys. 80 (1984) 4403–4409.
[52] H. Matsumoto, T. Sakata, H. Mori, H. Yoneyama, J. Phys. Chem. 100 (1996) 13781–13785.
[53] S. Baskoutas, A. Terzis, J. Appl. Phys. 99 (2006) 013708.
[54] C. Yang, Q. Jiang, Mater. Sci. Eng. B 131 (2006) 191–194.
[55] P. Lippens, M. Lannoo, Phys. Rev. B 39 (1989) 10935–10942.
[56] V. Fonoberov, E. Pokatilov, A. Balandin, Phys. Rev. B 66 (2002) 085310.
[57] S.V. Gaponenko, Optical Properties of Semiconductor Nanocrystals, University Press, Cambridge, 1998.
[58] K. Nanda, F. Kruis, H. Fissan, Nano Lett. 1 (2001) 605–611.
[59] Landolt-Börnstein (*Numerical data and functional relationships in science and technology*) – Group III: Condensed Matter, section 2.1.26 (Cadmium sulfide), p. 88.
[60] E. Silvester, F. Grieser, B. Sexton, T. Healy, Langmuir 7 (1991) 2917–2922.
[61] K. Drummond, F. Grieser, T. Healy, E. Silvester, M. Giersig, Langmuir 15 (1999) 6637–6642.
[62] M. Brelle, C. Torres-Martinez, J. McNulty, R. Mehra, J. Zhang, Pure Appl. Chem. 72 (2000) 101–117.
[63] A. Raevskaya, A. Stroyuk, S. Kuchmiy, A. Kryukov, J. Mol. Catal. A 212 (2004) 259–265.
[64] Y. Wang, A. Suna, W. Mahler, R. Kasowski, J. Chem. Phys. 87 (1987) 7315.
[65] H. Miyoshi, M. Yamachika, H. Yoneyama, H. Mori, J. Chem. Soc., Faraday Trans. 86 (1990) 815–818.
[66] L. Cademartiri, E. Montanari, G. Calestani, A. Migliori, A. Guagliardi, G. Ozin, J. Am. Chem. Soc. 128 (2006) 10337–10346.
[67] I. Kang, F. Wise, J. Opt. Soc. Am. B 14 (1997) 1632–1646.
[68] R. Kane, R. Cohen, R. Silbey, J. Phys. Chem. 100 (1996) 7928–7932.
[69] K. Nanda, F. Kruis, H. Fissan, S. Behera, J. Appl. Phys. 95 (2004) 5035–5041.
[70] V. Shvalagin, A. Stroyuk, S. Kuchmiy, Theoret. Exp. Chem. 43 (2007)215–219.
[71] C. Lee, J. Park, J. Phys. Chem. B 105 (2001) 2365–2368.
[72] M. Nenadović, M. Čomor, V. Vasić, O. Mićić, J. Phys. Chem. 94 (1990) 6390–6396.
[73] T. Torimoto, T. Sakata, H. Mori, H. Yoneyama, J. Phys. Chem. 98 (1994) 3036–3043.
[74] A. Kulak, Electrochemistry of Semiconductor Heterostructures (in russian), Universitetskoye, Minsk, 1986.
[75] M. Zhukovski, Yu. Gnatyuk, N. Smirnova, A. Eremenko, Chem. Phys. Technol. Surf. 13 (2007) 130–135.
[76] J. Yu, J. Yu, W. Ho, J. Zhao, J. Photochem. Photobiol. A 148 (2002) 331–339.
[77] N. Sakai, A. Fujishima, T. Watanabe, K. Hashimoto, J. Phys. Chem. B 105 (2001) 3023–3041.